PCCP

Stabilizing the crystal structures of NaFePO4 with Li substitutions

Journal:	*Physical Chemistry Chemical Physics*
Manuscript ID	CP-ART-02-2020-001056.R2
Article Type:	Paper
Date Submitted by the Author:	02-Jun-2020

Complete List of Authors:	Wang, Renhai; University of Science and Technology of China, Department of Physics Wu, Shunqing; Xiamen University, Department of Physics Zhang, Feng; Ames Laboratory Zhao, Xin; Ames Laboratory Lin, Zijing; University of Science and Technology of China, Department of Physics; Hefei National Laboratory for Physical Sciences at the Microscale, Wang, Cai Zhuang; Ames Laboratory-U.S. DOE, Physics and Astronomy Ho, Kai-Ming; Iowa State University,

Stabilizing the crystal structures of $NaFePO_4$ with Li substitutions

Renhai Wang,[a,b] Shunqing Wu,[c] Feng Zhang,[b] Xin Zhao,[b] Zijing Lin,[*a] Cai-Zhuang Wang,[b] Kai-Ming Ho,[*b,d]

[a]*Department of Physics, University of Science and Technology of China, Hefei 230026, China*

[b]*Ames Laboratory, US DOE and Department of Physics, Iowa State University, Ames, Iowa 50011, United States*

[c]*Department of Physics, OSED, Key Laboratory of Low Dimensional Condensed Matter Physics (Department of Education of Fujian Province), Jiujiang Research Institute, Xiamen University, Xiamen 361005, China*

[d]*International Center for Quantum Design of Functional Materials (ICQD), Hefei National Laboratory for Physics Sciences at the Microscale, University of Science and Technology of China, Hefei 230026, China*

Abstract

Due to the high cost and insufficient resource of lithium, alternative sodium-ion batteries are widely investigated for large-scale applications. $NaFePO_4$ has the highest theoretical capacity of 154 mAh g^{-1} among the iron-based phosphates, which makes it an attractive cathode material for Na-ion batteries. Experimentally, $LiFePO_4$ has been highly successful as cathode in Li-ion batteries because its olivine crystal structure provides a stable frame work during battery cycling. In $NaFePO_4$, maricite replaces olivine as the most stable phase. However, the maricite phase is experimentally found to be electrochemically inactive under normal battery operating voltages (0-4.5 V). We found that partial substitutions of Na with Li stabilize the olivine structure and may be a way to improve the performance of $NaFePO_4$ cathodes. Using previously developed structural $LiFePO_4$ database, we examined the low-energy crystal structures in the system when we replace Li with Na. The known maricite and olivine $NaFePO_4$ phases are reconfirmed and an unreported phase with energy between them is identified by our calculations. Besides, the Li-doped olivine type compound $Li_xNa_{1-x}FePO_4$ with mixed alkali ions retain better energetic stability than the other two types of structures of the same composition, as long as the proportion

* Email: kmh@iastate.edu (K.H.) or zjlin@ustc.edu.cn (Z.L.)

of Li exceeds 0.25. The thermodynamic stability of o-type $Li_xNa_{1-x}FePO_4$ can be further improved at finite temperatures. The primary limitation of the calculations is we mainly focus on the zero temperature condition; however the relative stability of the structures may vary depending on the ambient temperature.

1. Introduction

Large-scale energy storage systems for grids are extremely important for the storage and utilization of the renewable resources, such as solar and wind power[1, 2]. Currently, lithium-ion batteries (LIBs) have become the most widely used devices for energy storage[3, 4] to satisfy the demand of different grid functions[5]. However, the applications of LIBs in large-scale energy storage are limited by the high cost and limited availability of lithium[6]. Compared to LIBs, sodium-ion batteries (SIBs) are cheaper due to the low cost and abundance of sodium in the earth, making NIBs suitable for large-scale energy storage devices where high energy density becomes less critical[7].

Over the past decade, extensive academic investigations in SIBs have been focused on the development of cathode materials[1, 8-10]. Using the knowledge obtained during the extensive research of the Li-ion battery materials, potentially useful materials can be prepared both as lithium or sodium analogues[11, 12]. Polyanion phosphate cathode materials are promising candidates owing to their relatively high operating potentials and thermal stability. In particular, olivine $NaFePO_4$ (o-NFPO) has the highest theoretical specific capacity (154 mA h g^{-1})[13, 14], which makes it an attractive cathode material for SIBs. However, the complexity of the fabrication process impedes its application. Olivine $LiFePO_4$ has been very successful as a cathode material because it has one-dimensional channels for Li diffusion. However, o-NFPO is

not favored in the sodium analogue[12, 15]. The thermodynamically stable maricite $NaFePO_4$ (m-NFPO) has been experimentally found to be electrochemically inactive under normal battery operating voltages (0-4.5 V) because cavities with trapped Na ions are not connected by pathways in the maricite structure[16]. Active $NaFePO_4$ cathodes need to be fabricated in the metastable olivine phase and operated at low temperatures since Avdeev et al.,[15] reported that the $NaFePO_4$ system exhibits an irreversible phase transition from o-NFPO to m-NFPO around 480 ℃ by variable-temperature X-ray diffraction patterns analysis.

In this study, we managed to extend the existing database by replacing the element Li with Na in the previously established $LiFePO_4$ crystal structures (LFPOs) database[17]. This database has effectively explored the low energy structures of $LiFeSiO_4$ system[18]. In this way, we get many low-energy structures that far exceed the Materials Project[19] (MP) database. The known maricite and olivine $NaFePO_4$ phases are reconfirmed and an unreported phase with energy between m-NFPO and o-NFPO is discovered. Here, we do a comparison of the formation energy of the three different types of NFPOs doped with different ratios of Li. We found that the olivine type structure of the mixed alkali ion compound $Li_xNa_{1-x}FePO_4$ is more stable in energy comparing to the other two types of structures when the proportion of Li exceeds 0.25. In this paper, we mainly focus on the zero temperature condition. And the relative stabilities of the structures could be different for ambient temperature. But our results are still valuable and meaningful.

2. Computational Methods

The present calculations are based on the spin-polarized density functional theory (DFT) and the Vienna Ab initio Simulation Package (VASP)[20, 21] with the projector-augmented wave (PAW)[21] representations. The Perdew-Burke-Ernzerhof (PBE)[22] exchange-correlation functional

is used, together with the Hubbard U corrections (GGA+U) in the rotationally invariant form introduced by Dudarev et al[23]. to address the self-interaction energy. Considering the strong electron correlation effects, the U–J parameters were applied as the same as those adopted by LFPOs database[17]. An effective Ueff = U − J = 4.3 eV is used for Fe atoms. Also, magnetic ions (Fe) were initialized ferromagnetically. Brillouin-zone integrations are approximated by using special $\boldsymbol{k}$-point sampling of Monkhorst-Pack scheme[24] with a $\boldsymbol{k}$-point mesh resolution of $2\pi \times 0.03$ Å^{-1}. The wave functions are expanded by using the plane waves up to a kinetic energy cutoff of 520 eV. The unit cell lattice vectors (both the unit cell shape and size) are fully relaxed together with the atomic coordinates until the force on each atom is less than 0.01 eV/Å. Crystal structure figures are plotted using VESTA[25]. Phonon density of states calculations were performed using the finite difference method via the Phonopy code[26]. The energy cutoff was 520 eV and the convergence criterion for the total energy was set to 10^{-8} eV.

Three low-energy FeO_6 type $NaFePO_4$ crystal structures consist of 4 f.u. per unit cell. In the study of Li-doping in these structures, we doubled the unit cell so that the doping ratios of Li can be covered: 12.5%, 25%, 37.5%, 50%, 62.5%, 75% and 87.5%. We considered all possible doping sites and calculated the formation energy (eV/f.u.) of corresponding structures using the following formula:

$$E_f(Li_xNa_{1-x}FePO_4) = E(Li_xNa_{1-x}FePO_4) - x * E(LiFePO_4) - (1-x) * E(NaFePO_4), \quad (1)$$

where $E(Li_xNa_{1-x}FePO_4)$ is the energy of $Li_xNa_{1-x}FePO_4$ (eV/f.u.), $E(LiFePO_4)$ and $E(NaFePO_4)$ are the energy of ground state olivine-phase of $LiFePO_4$ and ground state maricite-phase of $NaFePO_4$, respectively.

3. Results and Discussion

Our initial structures of NFPOs come from the low-energy LFPOs database previous set up using Fe-P networks schemes[17]. NFPOs are obtained by substituting Li in low-energy structures in the LFPOs database with Na. **Figure 1** compares the energy of individual low-energy structures before and after substitution. The energies for NFPOs and LFPOs are referenced to their respective ground state. Different markers show different types of Fe-O polyhedra in the resulting of NFPOs. In addition, a red dotted line with a slope of 1.0 is used as a reference. It can be seen from **Figure 1** that most structures are located in the upper half of the dotted line with a slope of 1, which means that the relative formation energy of most structures is reduced after the LFPO-NFPOs transformation.

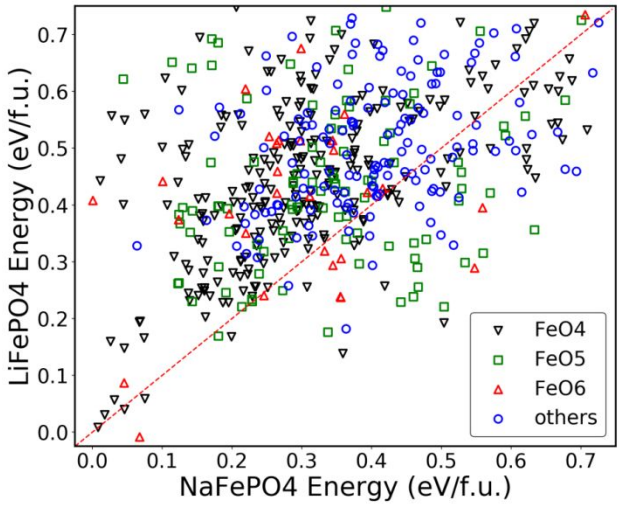

Figure 1 Correlations between the energy of $NaFePO_4$ and their source $LiFePO_4$ structures. In the energy, the value is relative to the ground state of each type ($LiFePO_4$ and $NaFePO_4$). Polyhedra with different coordination numbers (CN) of Fe-O in the $NaFePO_4$ structures are plotted with different colors and shapes.

In Figure S1 (see supplementary materials), we show the changes in the structure of two lower-energy structures with FeO_4 type. The lowest energy structure of FeO_4 type shows good correspondence between NFPOs and LFPOs in terms of energy order and structure.

3.1 Low energy window of $NaFePO_4$

The energy window of 0.35 eV/f.u corresponds to proximately 600 K in terms of temperature, which is the most relevant energy window for battery applications. We replotted the energies within 0.35 eV/f.u of the DFT-relaxed structures against their corresponding volumes, shown in **Figure 2**. It can be seen that the low energy structures under 0.15 eV/f.u. are separated by the volume of about 90 $Å^3$/f.u., which correspond to FeO_6 structures and FeO_4 structures, respectively. Both experimentally observed structures are at the smaller volume valley, corresponding higher energy density. As shown in the small black and red boxes in **Figure 2**, our results successfully recovered the two structures reported in experiments, which are maricite type (marked as m-type) and olivine type (marked as o-type) with FeO_6 motif. In Ref.[15], Avdeev, et al. reported the m-type and o-type structures. They showed the lattice of m-type were 8.976, 6.868 and 5.043 Å with a space group Pnma, which is consistent with our m-type parameter of 9.113, 6.934 and 5.108 Å (see Table S1). And the lattice of o-type were 10.401, 6.218 and 4.946 Å with a space group Pnma, which is also consistent with our o-type parameter of 10.551, 6.321 and 4.999Å (see Table S2). In order to further compare the m-type and o-type structures with the experimental structures, we relaxed the two experimental structures with VASP and plotted the energy-volume curves for comparison. It can be seen from Figure S2 (a) that the m-type and o-type we obtained almost coincide with the two points of the experimental structures. With these evidences, we believe that the known maricite and olivine $NaFePO_4$ phases are reconfirmed by our method. We also identified an unreported phase (marked as n-type in the green box in **Figure 2**, see Table S3 for detailed crystal information), whose energy is between the two known structures. This new phase also contains FeO_6 polyhedra.

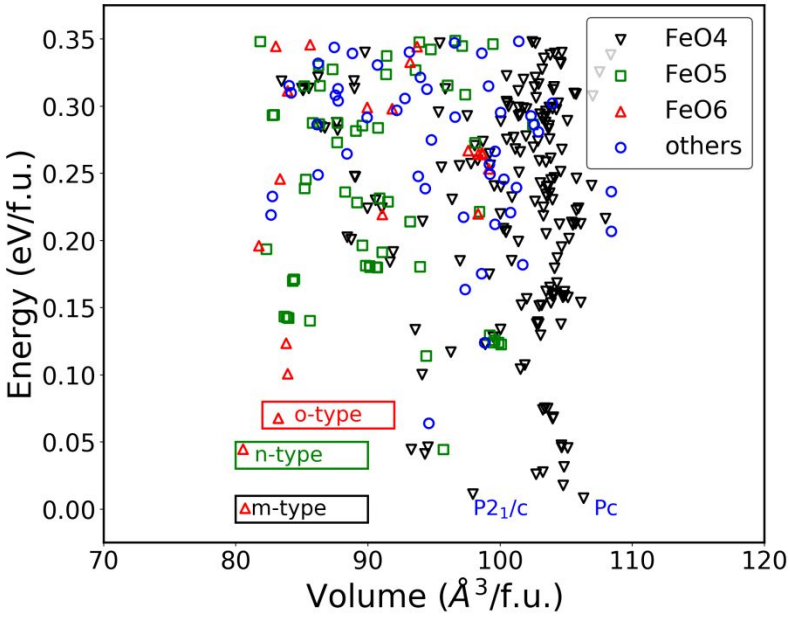

Figure 2 Energy vs. volume plot of the $NaFePO_4$ structures in our database get from $LiFePO_4$. Small black rectangle denotes the maricite type structure; small red rectangle denotes the olivine type structure; and small green rectangle denote the new type structure with FeO_6.

In order to check the validity of the value of U-J in this work, we repeated the DFT calculation with different value of U-J for five low-energy phases (m-type, n-type, o-type, Pc and $P2_1/c$, marked in **Figure 2**). A series of effective Ueff = U − J = 0.0, 1.3, 2.3, 3.3, 4.3, 5.3 eV are used for Fe atoms, in which 0.0 means only DFT calculation without U. As shown in **Figure S3**, only when the value of U-J is equal to 4.3 or 5.3, the energy of m-type structure is the lowest. And we know that m-type is the ground state structure of NFPOs. Here we also keep the same value as the U-J value used in the calculation of the LFPOs system, so the value of U-J with 4.3 is reasonable.

3.2 Three low energy type of $NaFePO_4$ with FeO_6 polyhedra

Since the most widely used LFPO structures all have FeO_6 polyhedra, we focus on the three low-energy NFPOs that also contain FeO_6 in order to explore the feasibility of using NFPO structure as SIBs. **Table 1** gives the energy of three individual low-energy NFPOs and their

source LFPOs. The m-type NFPO is derived from a high-energy LFPO phase, the o-type NFPO is derived from the α-phase, which is the ground state of LFPO, and the n-type NFPO structure is obtained from β-phase, which is a high-pressure and high-temperature phase of LFPO. All three parent LFPO structures also have FeO_6 motifs. **Figure 3** compares the atomic structures of the three types of NFPO and their corresponding LFPOs. The structures of o-type NFPO and LFPO are consistent, which also explains why the experimental olivine $NaFePO_4$ was obtained from olivine $LiFePO_4$ via chemical delithiation and followed by sodiation[27]. The crystallographic details, including space groups, lattice parameters, Wyckoff site and atomic coordinates, are given in Supplemental Materials. It should be noted that when Na is changed back to Li in m-NFPO, it results in a new LFPO structure with energy of 0.196 instead of the original high energy LFPO structure with energy of 0.408. When in the other two cases, the transition from LFPO to NFPO is reversible. This result shows that the structure database of the LFPOs we established before is not perfect enough, but as long as the data coverage is wide enough, we can still get very meaningful results.

To examine the stability of the three type NFPO structures from our database, we calculated the phonon density of states using the frozen phonon method. The m-type and o-type structures were expanded using a 1 x 2 x 2 supercell (112 atoms). The n-type structure was not expanded (28 atoms). **Figure 4** shows the phonon density of states of these structures, where it can be seen that all three structures are dynamically stable.

Table 1 The energy order between the NFPO and their source LFPO of three FeO_6 types NFPOs.

Structures and energy	NFPO		
	o-type 0.068	n-type 0.045	m-type 0.0
Corresponding LFPO and energy	α 0.0	β 0.087	other 0.408

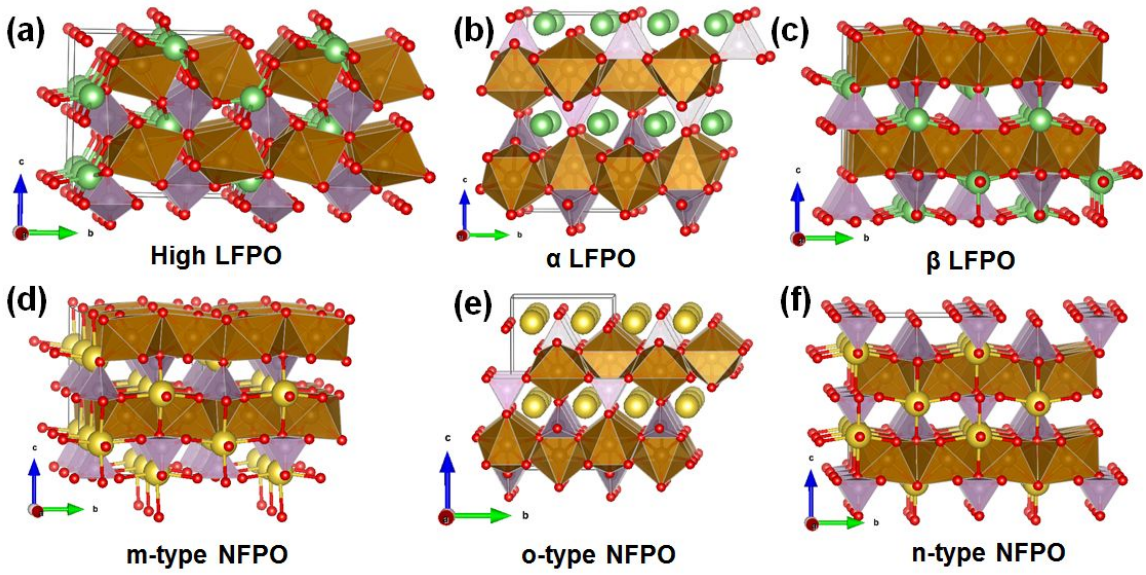

Figure 3 Phase relationship between LFPO phases and NFPO phases. Atom color: Li, Na, Fe, P, and O atoms colored with green, yellow, brown, purple and red, respectively.

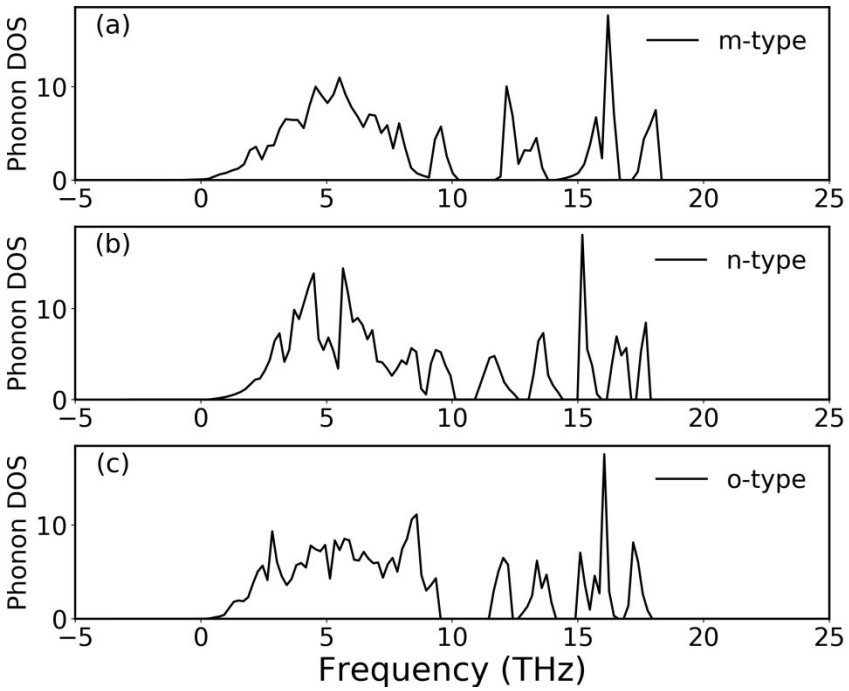

Figure 4 Phonon density of states of m-type, n-type and o-type $NaFePO_4$ structures.

3.3 $Li_xNa_{(1-x)}FePO_4$ (x = 0.125, 0.25, 0.375, 0.5, 0.625, 0.75)

As we know, the olivine $NaFePO_4$ could not be easily synthesized by conventional method of solid-state reaction for the main reason that the ionic radius of Na^+ (1.02 Å) is 55% larger than

that of Li^+ (0.76 Å). Based on the above analysis of the structure and energy order of o-NFPO and o-LFPO, we hypothesized that we should be able to find "good structure" (similar to o-LFPO) with low-energy order by doping Li atoms in the Na atoms sites of different NFPOs. Then, we selected the three types (o-type, m-type and n-type) of NFPOs in **Figure 3** to do doping with different ratios of Li, forming $Li_xNa_{(1-x)}FePO_4$ (x = 0.0, 0.125, 0.25, 0.375, 0.5, 0.625, 0.75, 0.875, 1.0) structures. The relationship between the formation energy calculated according to Eq. (1) and the doping ratio of Li is shown in **Figure 5**. It can be seen that the olivine structures have the lowest energy when the Li doping ratio exceeds 25%. In other words, doping with Li can effectively destabilize the maricite structure and stabilize the olivine structure, which could be an efficient way to improve the performance of NFPO. Nonetheless, these results must be interpreted with caution, and it should be borne in mind that we mainly focus on the zero temperature condition, however the relative stabilities of the structures could be different for ambient temperature.

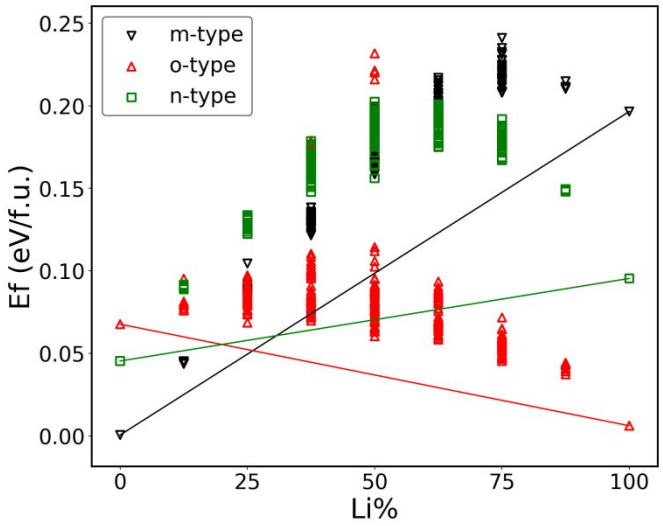

Figure 5 Formation energy of Li-doped $Li_xNa_{(1-x)}FePO_4$ (x = 0, 0.125, 0.25, 0.375, 0.5, 0.625, 0.75, 1.0) composites of three different types (m-type, o-type and new-type) of NFPOs. In the energy, the value is relative to the ground state of α-$LiFePO_4$ and m-$NaFePO_4$.

The calculation of the Gibbs free energy at high temperature is very necessary to evaluate the stability of the structures. Here, the thermal properties for three types NFPO and the lowest energy $Li_{0.25}Na_{0.75}FePO_4$ structures are calculated from phonon frequencies within the harmonic approximation. The curve of entropy vs. temperature for m-type, o-type and n-type structures is shown in **Figure 6** (a). It can be seen that the m-type NFPO structure have always maintained a lower entropy value than the other two types of structures at high temperatures. **Figure 6** (b) shows the dissociation energies for $Li_{0.25}Na_{0.75}FePO_4 \rightarrow 0.75NaFePO_4 + 0.25\mathrm{Li}FePO_4$, and the $E_f = E(Li_{0.25}Na_{0.75}FePO_4) - 0.25E(\mathrm{Li}FePO_4) - 0.75E(NaFePO_4)$. The results show that when the temperature is higher than 100K, the dissociation energy of $Li_{0.25}Na_{0.75}FePO_4$ is less than zero, which means that the structure becomes thermodynamically stable.

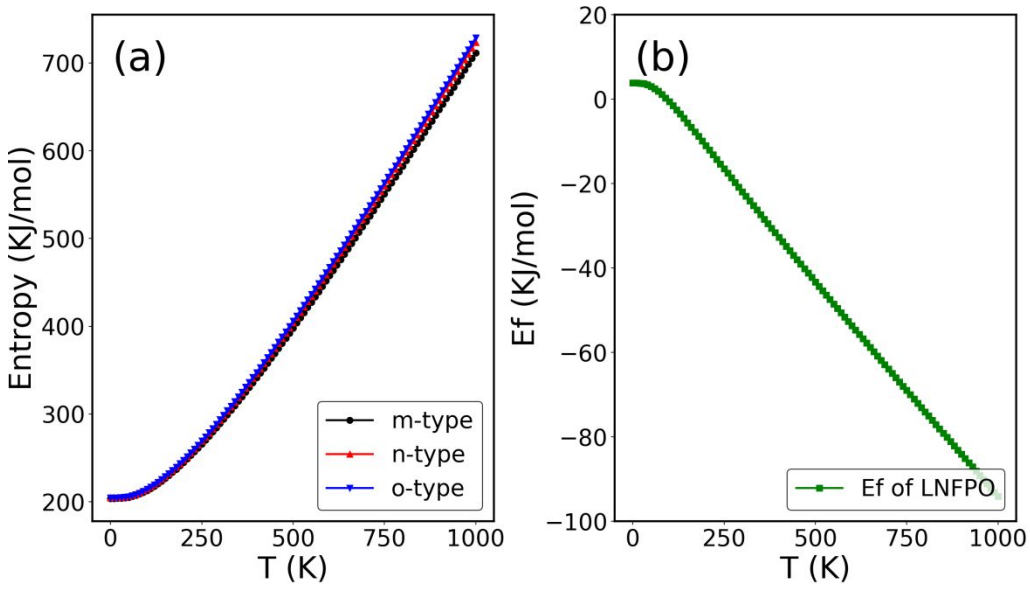

Figure 6. Thermal properties for three type NFPOs and $Li_{0.25}Na_{0.75}FePO_4$. (a): Entropy vs. temperature for m-type, o-type and n-type structures; (b): the dissociation energies for $Li_{0.25}Na_{0.75}FePO_4 \rightarrow 0.75NaFePO_4 + 0.25\mathrm{Li}FePO_4$.

In **Figure 7**, we give the snapshot of $Li_{0.25}Na_{0.75}FePO_4$ and $Li_{0.375}Na_{0.625}FePO_4$, which are doping from the o-type NFPO. It can be seen that both structures maintain the olivine type.

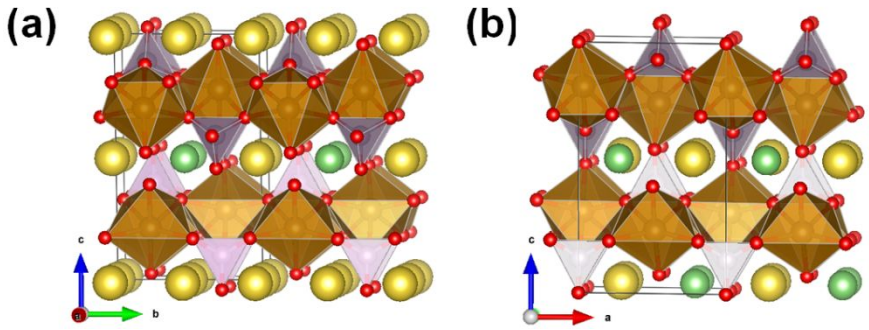

Figure 7. Structural snapshot of $Li_{0.25}Na_{0.75}FePO_4$ and $Li_{0.375}Na_{0.625}FePO_4$ from o-type NFPO.

We can use the equation (2) to evaluate the theoretical capacity of a given electrode material:

$$C^{theo} = 26.8 \times \frac{1}{M} \times \Delta z \ \ (Ahg^{-1}), \quad (2)$$

where *M* is Molar mass of the compound, while Δz is the number of electrons that can participate in the reaction. According to the equation, the highest theoretical specific capacity of $LiFePO_4$ and $NaFePO_4$ are 170 and 154 mAh g^{-1}, respectively.

If only the (de-)intercalation of Na ions is counted and the entire Na ion in the structure can be extracted, then the maximum theoretical capacity of $Li_xNa_{1-x}FePO_4$ is:

$$C^{theo} = 26.8 \times \frac{1}{M(Li_xNa_{1-x}FePO_4)} \times (1-x) \quad (Ahg^{-1}), \quad (3)$$

Here we concerned with the composition of Li-doped NFPO with a ratio of Li in the range of 0.25 to 0.5, so the theoretical specific capacity of the three components $Li_{0.25}Na_{0.75}FePO_4$, $Li_{0.375}Na_{0.625}FePO_4$ and $Li_{0.5}Na_{0.5}FePO_4$ are 118, 100 and 81 mAh g^{-1}, respectively.

In order to explore whether Li ions will become cations in the electrochemical cycling process of NFPO electrode materials, we compared the vacancy formation energies for Li/Na ions at different stages. Here, we take one structure ($Li_{0.25}Na_{0.75}FePO_4$) as an example and calculate the vacancy formation energies during electrochemical process. Then we compare the following two processes:

$LiNa_3Fe_4P_4O_{16} \rightarrow Na + LiNa_2Fe_4P_4O_{16}$, (4)

$LiNa_3Fe_4P_4O_{16} \rightarrow Li + Na_3Fe_4P_4O_{16}$, (5)

For (4), the vacancy formation energy: $E_{f1} = [E(LiNa_2Fe_4P_4O_{16}) + E(Na) - E(LiNa_3Fe_4P_4O_{16})]/28$

For (5), the vacancy formation energy: $E_{f2} = [E(Na_3Fe_4P_4O_{16}) + E(Li) - E(LiNa_3Fe_4P_4O_{16})]/28$

According to our DFT calculation, the E_{f1}(0.0675 eV/atom) is lower than E_{f2}(0.1514 eV/atom), so the Na ions will preferentially participate in the electrochemical cycle process.

4. Conclusion

We developed an efficient element-replacing scheme to create new structures of NFPO based on an established LFPO database. A large number of undiscovered low-energy structures have been obtained, which allows us to build a relatively comprehensive crystal structure database for NFPOs for further study. We explored the energy landscape of the new NFPOs and divided the structures into two groups according to the volume and energy. By comparing the structures of NFPOs with those of the original LFPOs, it is found that the olivine type NFPO is derived from the olivine type LFPO and the ground state maricite type of NFPO is derived from a high-energy structure of LFPO. In addition, an unreported structure with FeO_6 motif is obtained from the high-pressure and high-temperature phase (β-phase) of LFPO, whose energy order is between the two experimentally reported structures (m-type and o-type). Based on the strong correlation between NFPOs and LFPOs, we study the doping of Li in three structures with FeO_6 polyhedra. The olivine type $Li_xNa_{1-x}FePO_4$ becomes more stable than the maricite type

when x > 0.25. Thermodynamic calculations within the harmonic approximation show that $Li_{0.25}Na_{0.75}FePO_4$ is stable at $T > 100$ K, suggesting that these compounds may be synthesized as a sodium-ion battery material at finite temperatures. There is one major limitation in this study that could be addressed in future research, which is we mainly consider the zero point calculation, but the relative stability of the structures may change due to the increase in ambient temperature.

Conflicts of interest

There are no conflicts to declare

Acknowledgments

Work at University of Science and Technology of China was supported by the National Natural Science Foundation of China (11574284 & 11774324) and the Supercomputing Center of USTC. R. Wang acknowledges the support from USTC and China Scholarship Council (File No. 201906340034). Work at Ames Laboratory was supported by the U.S. Department of Energy, Basic Energy Sciences, Materials Science and Engineering Division, under Contract No. DEAC02-07CH11358, including a grant of computer time at the National Energy Research Scientific Computing Center (NERSC) in Berkeley, CA. Work at Xiamen University was supported by the National Natural Science Foundation of China (11874307).

References

1. N. Yabuuchi, K. Kubota, M. Dahbi and S. Komaba, *Chemical reviews*, 2014, **114**, 11636-11682.
2. J. Yang, X. Zhou, D. Wu, X. Zhao and Z. Zhou, *Advanced Materials*, 2017, **29**, 1604108.
3. J.-M. Tarascon and M. Armand, in *Materials for Sustainable Energy: A Collection of Peer-Reviewed Research and Review Articles from Nature Publishing Group*, World Scientific2011, pp. 171-179.
4. Y. Zhong, M. Yang, X. Zhou, Y. Luo, J. Wei and Z. Zhou, *Advanced Materials*, 2015, **27**, 806-812.
5. B. Dunn, H. Kamath and J.-M. Tarascon, *Science*, 2011, **334**, 928-935.
6. J.-M. Tarascon, *Nature chemistry*, 2010, **2**, 510.
7. S. W. Kim, D. H. Seo, X. Ma, G. Ceder and K. Kang, *Advanced Energy Materials*, 2012, **2**, 710-721.

8. L. Yang, Y. E. Zhu, J. Sheng, F. Li, B. Tang, Y. Zhang and Z. Zhou, *Small*, 2017, **13**, 1702588.
9. Y. E. Zhu, L. Yang, J. Sheng, Y. Chen, H. Gu, J. Wei and Z. Zhou, *Advanced Energy Materials*, 2017, **7**, 1701222.
10. R. Berthelot, D. Carlier and C. Delmas, *Nature materials*, 2011, **10**, 74.
11. M. Pivko, I. Arcon, M. Bele, R. Dominko and M. Gaberscek, *Journal of Power Sources*, 2012, **216**, 145-151.
12. B. Ellis, W. Makahnouk, Y. Makimura, K. Toghill and L. Nazar, *Nature materials*, 2007, **6**, 749.
13. W. Tang, X. Song, Y. Du, C. Peng, M. Lin, S. Xi, B. Tian, J. Zheng, Y. Wu and F. Pan, *Journal of Materials Chemistry A*, 2016, **4**, 4882-4892.
14. Y. Zhu, Y. Xu, Y. Liu, C. Luo and C. Wang, *Nanoscale*, 2013, **5**, 780-787.
15. M. Avdeev, Z. Mohamed, C. D. Ling, J. Lu, M. Tamaru, A. Yamada and P. Barpanda, *Inorganic chemistry*, 2013, **52**, 8685-8693.
16. P. P. Prosini, C. Cento, A. Masci and M. Carewska, *Solid State Ionics*, 2014, **263**, 1-8.
17. X. Lv, X. Zhao, S. Wu, P. Wu, Y. Sun, M. C. Nguyen, Y. Shi, Z. Lin, C.-Z. Wang and K.-M. Ho, *Journal of Materials Chemistry A*, 2017, **5**, 14611-14618.
18. X. Lv, X. Zhao, S. Wu, M. C. Nguyen, Z. Zhu, Z. Lin, C.-Z. Wang and K.-M. Ho, *Physical Chemistry Chemical Physics*, 2018, **20**, 14557-14563.
19. A. Jain, S. P. Ong, G. Hautier, W. Chen, W. D. Richards, S. Dacek, S. Cholia, D. Gunter, D. Skinner, G. Ceder and K. A. Persson, *APL Materials*, 2013, **1**, 011002.
20. G. Kresse and J. Furthmüller, *Computational materials science*, 1996, **6**, 15-50.
21. G. Kresse and J. Furthmüller, *Physical review B*, 1996, **54**, 11169.
22. J. P. Perdew, K. Burke and M. Ernzerhof, *Physical review letters*, 1996, **77**, 3865.
23. S. Dudarev, G. Botton, S. Savrasov, C. Humphreys and A. Sutton, *Physical Review B*, 1998, **57**, 1505.
24. H. J. Monkhorst and J. D. Pack, *Physical review B*, 1976, **13**, 5188.
25. K. Momma and F. Izumi, *Journal of applied crystallography*, 2011, **44**, 1272-1276.
26. A. Togo and I. Tanaka, *Scripta Materialia*, 2015, **108**, 1-5.
27. F. Xiong, Q. An, L. Xia, Y. Zhao, L. Mai, H. Tao and Y. Yue, *Nano Energy*, 2019, **57**, 608-615.